Research Article

Gerardo A Lopez-Muñoz, Juan M Fernández-Costa, Maria Alejandra Ortega, Jordina Balaguer-Trias, Eduard Martin-Lasierra and Javier Ramón-Azcón*

Plasmonic nanocrystals on polycarbonate substrates for direct and label-free biodetection of Interleukin-6 in bioengineered 3D skeletal muscles

Abstract: The development of nanostructured plasmonic biosensors has been widely widespread in the last years, motivated by the potential benefits they can offer in integration, miniaturization, multiplexing opportunities, and enhanced performance label-free biodetection in a wide field of applications. Between them, engineering tissues represent a novel, challenging, and prolific application field for nanostructured plasmonic biosensors considering the previously described benefits and the low levels of secreted biomarkers ($\approx$pM–nM) to detect. Here, we present an integrated plasmonic nanocrystals-based biosensor using high throughput nanostructured polycarbonate substrates. Metallic film thickness and incident angle of light for reflectance measurements were optimized to enhance the detection of antibody–antigen biorecognition events using numerical simulations. We achieved an enhancement in biodetection up to 3× as the incident angle of light decreases, which can be related to shorter evanescent decay lengths. We achieved a high reproducibility between channels with a coefficient of variation below 2% in bulk refractive index measurements, demonstrating a high potential for multiplexed sensing. Finally, biosensing potential was demonstrated by the direct and label-free detection of interleukin-6 biomarker in undiluted cell culture media supernatants from bioengineered 3D skeletal muscle tissues stimulated with different concentrations of endotoxins achieving a limit of detection (LOD) of $\approx$ 0.03 ng/mL (1.4 pM).

Keywords: interleukin-6; label-free biosensing; plasmonic nanostructures; skeletal muscle; tissue engineering.

*Corresponding author: Javier Ramón-Azcón, Institute for Bioengineering of Catalonia (IBEC), The Barcelona Institute of Science and Technology, Baldiri I Reixac, 10-12, 08028 Barcelona, Spain; and ICREA-Institució Catalana de Recerca i Estudis Avançats, 08010 Barcelona, Spain, E-mail: jramon@ibecbarcelona.eu.
https://orcid.org/0000-0002-3636-8013
Gerardo A Lopez-Muñoz, Juan M Fernández-Costa, Maria Alejandra Ortega, Jordina Balaguer-Trias and Eduard Martin-Lasierra, Institute for Bioengineering of Catalonia (IBEC), The Barcelona Institute of Science and Technology, Baldiri I Reixac, 10-12, 08028 Barcelona, Spain. https://orcid.org/0000-0002-1854-6082 (J.M. Fernández-Costa)

1 Introduction

The increasing demand for high throughput analytical platforms that are reliable and, at the same time, versatile, highly sensitive, easy to use, and compact, have provided considerable innovation in the design of biosensor devices in the last years over a wide field of applications ranging from the development of point of care devices [1–3] to the development of platforms for biomarkers release detection in 2D and 3D cell cultures [4]. Related to the latter, *in vitro* 3D tissue models have the potential to study the physiological and pathological responses of biological processes in an easy, accurate, and controllable manner [5]. Remarkably, bioengineered 3D tissues have emerged as powerful tools for preclinical studies. As an example, drug screening platforms based on 3D muscle tissue models are promising tools to find treatments for muscular dystrophies [6, 7]. The detection of changes in biomarkers secretion is fundamental to understand the role of specific proteins in the regulation of biological processes and to study the evolution of a disease or the response to treatments in these preclinical platforms. However, the low levels of secreted proteins by *in vitro* 3D tissue models (usually in the pM–nM range) in complex cell culture media make challenging their direct detection [8] (Table 1).

Among all the biosensor devices, those based on plasmonic nanostructures have been the subject of great scientific interest because of the potential benefits they can offer in integration, miniaturization, multiplexing opportunities, simplicity in the detection schemes, and enhanced performance for direct and label-free bio-detection in a wide field of applications as the novel counterpart of the well-established plasmonic sensor [9]. However, to achieve fully operative nanostructured-based plasmonic biosensing platforms, several challenges must be surpassed, such as high throughput sensor fabrication techniques and nanostructures with enhanced surface sensitivity for low concentration/molecular weight analytes [9]. Although there have been some interesting approaches that try to solve some of these aspects, some of them either still require bulky detection schemes based on prism coupling [10, 11] or are based on complex and expensive fabrication processes, which limit their applicability outside the laboratory environment [12, 13]. Even more, only a limited number of approaches consider that bulk refractive index sensitivity, frequently used as a metric for performance, is not an appropriate benchmark for biosensing performance evaluation due to the divergence of the bulk and surface sensitivities [14–17].

Based on these considerations, we present a high throughput multichannel nanostructured plasmonic biosensor based on industrially produced Blu-ray as 1D nanocrystals containing substrates [18] for the sensitive, direct, and label-free detection of interleukin-6 in cell

Table 1: Comparison of different biosensing technologies for cytokine biodetection in cell culture.

Biodetection method	Type of assay	Limit of detection
Electrochemical [23]	Sandwich assay (2nd antibody)	(IL-6) 8 ng/mL
Magnetic+Electrochemical [4]	Labeled sandwich assay (2nd antibody)	(IL-6) 20 pg/mL
Electrochemical silicon nanowires [53]	Direct and label-free assay	(IL-4 and IL-2)- ≈ 39–65 fg/mL
Kretschmann SPR [24]	Sandwich assay (2nd antibody)	(IL-6) 1.3 ng/mL
Gold-capped nanopillars [26]	Direct and label-free assay	(IL-6) 10 ng/mL
Gold nanoparticles coated fiber optic [52]	Labeled sandwich assay (2nd antibody)	(IL-6) 1 pg/mL
Plasmonic nanocrystals[a]	Direct and label-free assay	(IL-6) ≈ 30 pg/mL

[a]This article.

culture supernatant from 3D skeletal tissues (see Figure 1). The present approach provides a high degree of controlled reproducibility while involving cost-effective fabrication, with a similar bulk refractive index sensitivity and a competitive biosensing performance compared to those obtained with engineered plasmonic nanocrystals [19–21]. In a first step, finite-difference time-domain (FDTD) numerical simulations were performed to optimize the metallic film thickness layer and the angle of incidence of light under reflectance detection scheme to enhance the plasmonic detection of antibody–antigen biorecognition events. The sensors were fabricated considering numerical simulations for optimal metallic film thickness layer with straightforward and reproducible processes. A multichannel polymethacrylate flow cell was used with patterned microfluidics obtained using a cost-effective medical-grade double-sided adhesive tape to achieve an integrated biosensor.

The sensors were optically characterized under transverse-magnetic (TM) polarized white light at different angles of incidence of light to evaluate their bulk sensitivity and biosensing performance, the last, using the insulin/anti insulin biorecognition event as a model to contrast the experimental results with numerical simulations with an increase up to 3× in biodetection at low incident angles of light; insulin was selected as a model due to their low molecular weight and low dimensions. Finally, the potential for biosensing was further explored in bioengineering 3D tissues. It was performed direct and label-free detection of interleukin-6 (IL-6) biomarker in undiluted cell culture media supernatants of bioengineered 3D skeletal muscle tissues based on encapsulated skeletal muscle myoblasts micropatterned hydrogels and stimulated with different concentrations of endotoxins (lipopolysaccharides). IL-6 is secreted by the damaged muscle tissue and activated leukocytes due to stimulating the innate immune system [22]. The secreted IL-6 concentration in cell culture media supernatants from 3D skeletal muscle tissues increased with endotoxins concentration in good agreement with previous reports [4, 23]. Finally, we achieve direct detection of IL-6 in undiluted cell culture media supernatants with a limit of detection (LOD) at least one order of magnitude better compared to other plasmonic and nanoplasmonic biosensing platforms [24–26], and similar to those obtained by electrochemical biosensing platforms using indirect detection (secondary antibody sandwich assay) [4, 23]. These results demonstrate the potential use of the presented biosensors for direct and label-free monitoring of secreted biomarkers in bioengineered 3D tissues and organoids.
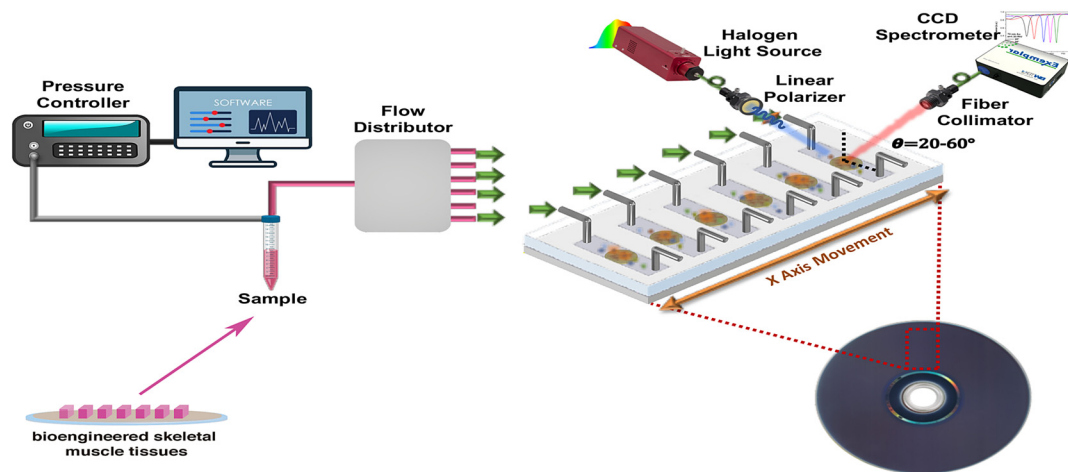
Figure 1: Schematic representation for developing a high throughput multichannel 1D plasmonic nanocrystals-based sensing platform for monitoring IL-6 levels in cell culture media supernatants from bioengineered 3D skeletal muscles.

2 Materials and methods

2.1 FDTD simulations

3D FDTD simulations were carried out using commercial software (FDTD solution, Lumerical, Inc., Vancouver, Canada). Structural parameters of the Blu-ray discs utilized in the simulations (i.e., a grating period of 320 nm, grating width of 100 nm, and a height of 20 nm) were as claimed to Atomic Force Microscopy (AFM) images from previous results [27]. Periodic boundary conditions were used on the x and y-axis, and the perfectly matched layers (PML) approach was used on the z-axis, with a uniform mesh size of 2 nm on all axes. The FDTD simulations were carried out in the range from 400 to 1000 nm under TM-polarized light with a variable oblique incidence angle of light (20–60°). The optical constants of the polycarbonate and gold were considered from Sultanova et al. [28] and Wakaki et al. [29], respectively. The refractive index of the biolayer was fixed to $n = 1.45$ RIU, according to previous reports [30].

2.2 Fabrication and integration of the 1D plasmonic nanocrystals chip

Single-layer recordable Blu-ray discs (43743, Verbatim, Taiwan) were used after the removal of their protective (thin polycarbonate) and reflective (aluminum) films. Reflective films were removed by cutting the disc in individual plasmonic chips (size 5.6 cm^2) and then immersed it in a hydrochloric acid solution (2 M HCl) overnight. Polycarbonate substrates were rinsed with deionized water and nitrogen dried. Sensing area chips were covered with a patterned adhesive vinyl stencil sheet (250 µm) as an evaporation mask placed in a vacuum deposition system (Univex 450B, Oerlikon Leybold, Germany). A 70 nm thick layer of gold was deposited by resistive thermal evaporation (1 Å/s). The microfluidic system for carrying out the biodetection in solution was developed using a patterned microfluidic multichannel in a 140 µm thick double-sided adhesive tape sheet (Mcs-foil-008, Microfluidic ChipShop GmbH, Germany). The proposed design integrates six individual channels with the potential for multiplexed

biodetection. A 2 mm tick patterned polymethyl methacrylate (PMMA) lid was added as a cover to facilitate the fluidic tubes' connection.

Chips were clamped to a custom-made optical platform for reflectance measurements. The chips were connected to a microfluidic pressure pump (OB1 Mark I, Elveflow, France), with adjustable pumping speed guaranteeing a constant liquid flow. Reflectance measurements were performed under TM-polarization of a compact stabilized broadband light source (SLS201L, Thorlabs, Germany) at a variable angle that ranges from 20 to 60°. The incident excitation plane was perpendicularly aligned to the nanograting direction. The reflected light was collected and fiber-coupled to a compact charge-coupled device (CCD) spectrometer (Exemplar UV-NIR, BWTek, Germany). Reflectivity spectra were acquired every 1 ms, and 50 consecutive spectra were measured and averaged to provide the final spectrum. These acquisition parameters were selected to obtain the optimum signal-to-noise (S/N) ratio without significantly increasing the data acquisition time. Changes in the resonance peak position (λSPR) were tracked via peak analysis using Origin 2018 software (OriginPro, OriginLab Co., Northampton, USA). Reflection spectra were collected in water ($n = 1.3329$ RIU), and HCl solutions in water (ranging between 1.3426 and 1.3623 RIU) were used to determine the bulk refractive index sensitivity of the 1D plasmonic nanocrystals-based sensor.

2.3 Surface biofunctionalization of 1D plasmonic nanocrystals and antibody detection assays

Self assembled monolayer (SAM) formation (11-mercaptoundecanoic acid, MUA), (1-ethyl-4 (3-dimethylaminopropyl)) carbodiimide hydrochloride (EDC), and sulfo-N hydroxysuccinimide (s-NHS) for carboxylic groups activation and ethanolamine were acquired to Merck (Germany). Gold chips were cleaned and activated for surface functionalization by performing consecutive rinsing with ethanol and deionized water, drying with N2 stream, and finally by placing them in a UV ozone generator (ProCleaner, BioForce Nanoscience, USA) for 20 min. An alkanethiol self assembled monolayer (SAM) with reactive carboxylic groups was obtained by coating the sensor chip with 2.5 mM MUA in ethanol overnight at room temperature. Then, the surface was rinsed with ethanol and carefully washed with MES buffer.

Immobilization of the insulin/interleukin-6 antibodies was performed ex-situ. Activation of the carboxylic groups were performed using a solution of 0.2 M EDC/0.05 M sulfo-NHS in (2-ethanesulfonic acid) MES buffer (25 mM pH 5.7) for 40 min. After washing steps using MES buffer, 50 µg/mL of mouse insulin (NB100-73008, Novus Bio, USA)/interleukin-6 (554400, BD Pharmingen, USA) antibody solution in (phosphate buffer) PB (10 mM pH 7.4) was dropped for 120 min. Furthermore, the sensor was submerged on an ethanolamine solution 50 mg/mL prepared in PB 10 mM pH 7.2 for 15 min to block unreacted remaining active carboxylic groups. Later washing steps using 2 mM HCl and PBS+0.1% BSA were performed to remove excess ligand and ethanolamine that is noncovalently bound and fill nonspecific binding sites. Finally, sensing areas were dried with an N_2 stream and bonded to the microfluidic channels, and placed in the optical platform, and filled with PBS for optimization and assessment studies.

Different IL-6 protein (200-02, Shenandoah Biotech, USA) concentrations diluted in Dulbecco's Modified Eagle Medium (DMEM) cell culture media flowed over the functionalized surface at 30 µL/min. Calibration curves were fitted to a one-site specific binding model. Data points for each concentration were collected 30 min after injection. A fixed concentration (250 ng/mL) of insulin protein (91077-C, Merck, Germany) in PBS (10 mM pH 7.4) was flowed over the functionalized surface to contrast the experimental results with the numerical simulations at different incident angles of light using the insulin/anti insulin model.

2.4 Cell culture

Murine C2C12 skeletal muscle myoblasts (ATCC, CRL-1772) were grown in Dulbecco's Modified Eagle Medium (DMEM, 4.5 g/L glucose, Gibco) supplemented with 1% penicillin–streptomycin (P/S, 10,000 U/mL, Thermofisher) and 10% fetal bovine serum (FBS, Gibco) at 37 °C and in a 5% CO_2 atmosphere. To induce differentiation into myotubes, the medium was changed to a differentiation medium, consisting of DMEM, supplemented with 2% horse serum (Thermofisher) and 1% penicillin/streptomycin.

2.5 Prepolymer preparation

Gelatin methacryloyl (GelMA) and carboxymethyl cellulose methacrylate (CMCMA) were synthesized as previously described in [31]. Both prepolymer and the photoinitiator lithium phenyl (2,4,6-trimethylbenzoyl) phosphinate (LAP, TCI Europe N.V.) were dissolved in MDM at 65 °C for 2 h. The concentrations of GelMA, CMCMA and LAP were fixed to obtain final concentrations of 5%, 1% and 0.1% (w/v), respectively.

2.6 Cell encapsulation in 3D microstructured hydrogels

Cell-laden 3D microstructured hydrogels were fabricated on top of PEGDA-coated glass coverslip using a photomold patterning technique, as described in [7]. Briefly, to encapsulate cells in micropatterned hydrogels, we mixed the prepolymer solution with a cell suspension in a growth medium to obtain a final concentration of 2.5×10^7 cells mL^{-1}. Then, an 8 µL drop of the cell-laden prepolymer was placed on a PEGDA-coated glass coverslip, and a PDMS stamp was pressed lightly on top, filling the microchannels with the solution. The hydrogels were crosslinked by UV exposure of 30 s using the UVP Crosslinker. MDM was added to each sample, and stamps were carefully removed after 20 min of incubation at 37 °C. Two days after cell encapsulation, the medium was replaced with a differentiation medium to induce myotubes maturation. Encapsulated cells were differentiated for up to 10 days, with culture media being replaced every two days.

2.7 Immunofluorescence staining

Bioengineered muscle tissues were fixed with 10% formalin solution (Sigma-Aldrich) for 30 min at room temperature (RT), followed by several washes in PBS. Samples were then permeabilized with PBS-T (0.1% Triton-X [Sigma-Aldrich] in PBS), blocked (0.3% Triton-X, 3% donkey serum [Sigma-Aldrich] in PBS) for 2 h at RT, and incubated with 1:200 anti-SAA primary antibody (Sigma-Aldrich) at 4 °C overnight. After several PBS-T washes, the samples were incubated for 2 h with the Alexa fluor-488-conjugated anti-mouse secondary antibody (Invitrogen) at RT. Finally, the samples were counterstained with DAPI (4′,6-diamidino-2-phenylindole, Life Technologies) to detect the nuclei. Fluorescence images were taken as Z-stacks with a ZEISS LSM800 confocal laser scanning microscope.

2.8 Lipopolysaccharide stimulation assay

To evaluate the effect of lipopolysaccharide (LPS) in IL-6 secretion, bioengineered 3D skeletal muscle microtissues were treated with different concentrations of LPS diluted in a differentiation medium. Encapsulated cells were differentiated for 7 days, then 3D microtissues were treated with LPS at 0.5, 1, and 10 µg mL^{-1} for 48 h. Cell supernatants were analyzed with our nanostructured plasmonic biosensor using the differentiation medium as a control. Three replicas for each condition were analyzed.

2.9 Limit of detection (LOD) and working range (WR) estimation

The standard curves were fitted to a four-parameter equation according to the following formula: $Y = [(A - B)/1 - (x/C)^D] + B$ where A is the maximal signal, B is the minimum, C is the concentration producing 50% of the maximal signal, and D is the slope at the inflection point of the sigmoid curve. The calculation of parameters of the calibration curve was based on analytical methodology [32]. For a standard curve, the LOD was calculated based on the value of three times the standard deviation of the value of the lowest concentration. The biosensor's working range (WR) was calculated considering the antigen concentration range between 10 and 90% of the dynamic signal range, according to Chiavaioli et al. [33]. The software used for this fitting and statistics was GraphPad Analysis Software using a dose–response four-parameter fitting model. All the measurements were performed in duplicate.

3 Results and discussion

3.1 Simulation, fabrication, and characterization of 1D plasmonic nanocrystals.

In order to optimize the metallic film thickness layer and the angle of incidence of light under a reflectance detection scheme to enhance the plasmonic detection of antibody–antigen biorecognition events, we perform optical simulations. Figure 2 summarizes FDTD simulation results. Metallic capped 1D plasmonic nanocrystals based on Blu-Ray disc nanostructured substrates were simulated using the FDTD method. Different gold thickness layers between 40 and 90 nm were simulated at a fixed 20° oblique incidence angle of light in a reflectance scheme under aqueous media (1.33 RIU). To determine the optimal gold layer thickness for the detection of antibody–antigen biorecognition events, a 10 nm biolayer (1.45 RIU) was added to the FDTD model. This biolayer thickness was estimated considering a nonoriented antibody immobilization (6–7 nm height) and a low dimension protein target (insulin ≈ 5.8 kDa and molecular diameter ≈ 3 nm) [34–36]. For bulk refractive index sensitivity estimation, a significative

refractive index change in aqueous media was simulated (Δn = 0.02 RIU, 1.35 RIU). As can be observed in Figure 2A, below a 50 nm gold thickness layer, the plasmonic reflectance spectra lose sharpness mainly due to the strong interaction of the plasmonic wave with the underlying substrate [27]. However, above 80 nm gold thickness layer, a substantial decrease in the plasmon–exciton coupling is observed. The maximum plasmon–exciton coupling is achieved with a gold layer around 60–70 nm. On the other hand, as can be observed in Figure 2B although the bulk refractive index sensitivity increases with the gold layer thickness, the maximum surface sensitivity is achieved with a layer around 65–70 nm. The latter agrees with previous reports: in plasmonic biosensors based on high-ordered nanostructures, bulk refractive index sensitivity diverges from surface sensitivity due to the presence of different photonic coupling effects (i.e., cavity coupling or diffractive coupling) [37]. Consequently, bulk sensitivity is not an appropriate benchmark for biosensing performance evaluation in this type of nanostructures [14–16, 37].

Once the gold layer thickness was optimized, to evaluate the optimal incident angle of light for the selected biolayer thickness, different incident angles of light between 20 and 60° were simulated. Figure 2C shows the
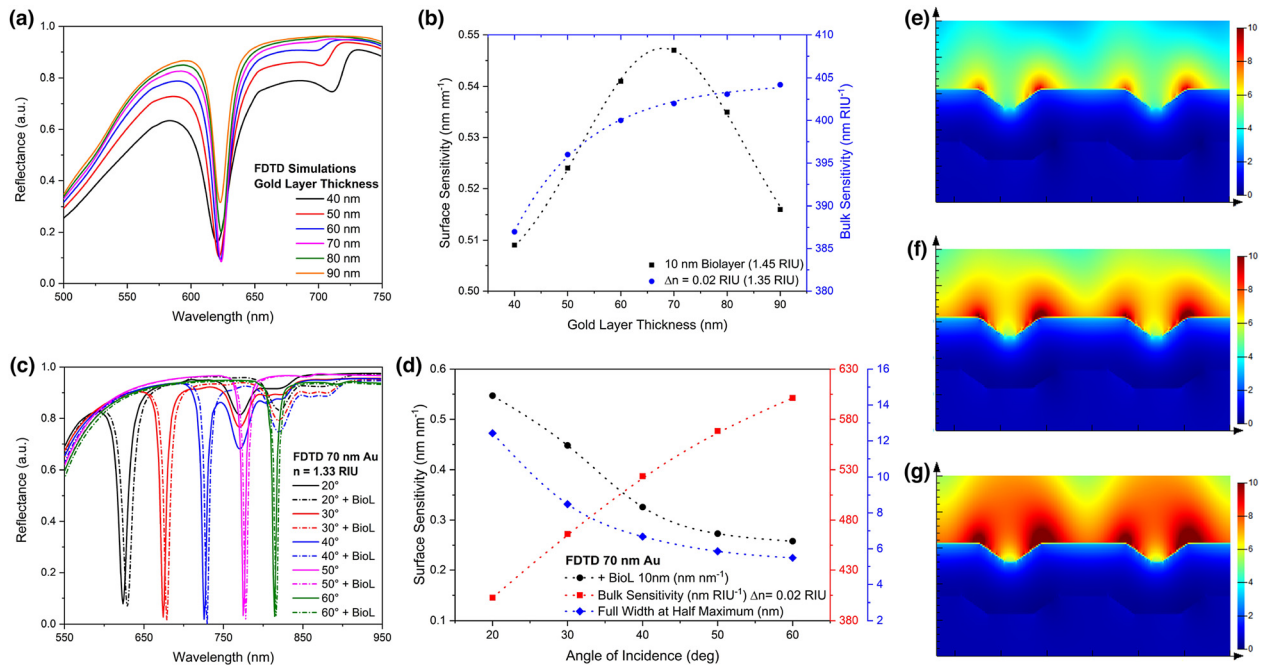

Figure 2: FDTD simulations of the proposed 1D plasmonic nanocrystals for optimized plasmonic biosensing.
(a) FDTD simulated reflectance under TM-polarization with a fixed light incident angle of 20° for different Au layer thicknesses. (b) Influence of the different Au thickness in the sensing and biosensing performance of the plasmonic nanostructures. (c) FDTD simulated reflectance change with the addition of a 10 nm biolayer under different light incident angles (20°–60°). (d) Influence of the different incident angles of light simulated in the sensing and biosensing performance of the plasmonic nanostructures. Simulated electric field distribution of the 70 nm Au coated plasmonic nanostructures under 20° (e), 40° (f), and 60° (g) light incidence angles.

reflectance spectra for a 70 nm gold layer thickness under different incident angles of light and the displacement of the plasmonic band with the addition of the 10 nm biolayer. As expected, as the incidence angle increases, the plasmonic band displace to the near-infrared region. This phenomenon can be described by the Bloch wave surface plasmon polariton mathematical model, when the Bragg condition for one-dimensional periodic metallic nanostructure is satisfied as has been previously described [18, 38, 39]. The observed decrease in the full width at half maximum (FWHM) of the plasmonic band under high incidence angles of light is related to the coupling of the native plasmonic resonances of the metallic nanostructures and surface lattice resonances due to the high ordered plasmonic nanocrystals behave as a grating [38, 40]. Increasing the angle of the incident light, the energy scattered from a nanostructure is collected by neighboring nanostructures, decreasing radiative losses and consequently narrowing and deepening the plasmonic bands [41]. The sensing results are summarized in the plots of Figure 2D. While there is an increase in bulk sensitivity with high incident angles of light, the surface sensitivity decreases. The last is related to the previously described; the decrease of radiative losses with high incident angles of light increases the evanescent field penetration length, enhancing the bulk refractive index sensing performance. On the other hand, as biomolecules are usually detected at a close distance to the surface, this extended evanescent field penetration length can diminish their performance [42, 43]. The latter can be observed in Figure 2E–G with an increase in the intensity of the electric-field distribution and the evanescent field penetration length as the incident angle of light increases. Different biolayer thicknesses were simulated under different incident angles of light to analyze the influence of extended evanescent field penetration lengths in the biosensing performance of the presented plasmonic nanostructures. S1A and B show the displacement of the plasmonic band under 20 and 40° incident angles of light with biolayer thicknesses in a range of 10–90 nm. As summarized in Figure S2A, the shift of the plasmonic band ($\Delta\lambda$) decreases at high incident angles of light. However, applying the first derivative to the curves in Figure S2A, it is observed in Figure S2B that high incident angles of light can improve the biodetection on tick biolayers (≥60 nm) due to the extended evanescent field decay length. This extended decay length at high incident angles of light could be helpful in the biodetection of larger bio targets (i.e., viruses or exosomes) [37].

Considering the FDTD simulations results, metallic capped 1D plasmonic nanocrystals were fabricated with a 70 nm gold thickness layer taking advantage of the precise and large area of nanostructured array present in commercial Blu-ray discs and the excellent adhesion of gold to polycarbonate, eliminating the use of adhesive layers (i.e., Ge, Cr or Ti) that can diminish the plasmon–exciton coupling by increased Ohmic plasmon losses [27]. As it is shown in Figure 3A, individual sensing areas were fabricated to allow multiple assays per chip. The diffraction of light and scanning electron microscopy (SEM) image in Figure 3B demonstrate the presence of high-ordered capped gold nanostructures. The sensors were characterized using the variable angle reflectance experimental set-up shown in Figure 3C. As shown in Figure 3D, similar behavior is observed between the FDTD simulations and the experimental reflectance spectra of the fabricated plasmonic nanocrystals with a displacement to the near-infrared region and a narrowing of the plasmonic band with high incident angles of light. The differences in the resonance peaks between the simulated and fabricated nanocrystals are mainly due to geometrical differences in the simulations (nanocrystals are radial to the Blu-ray disc's circumference, differences in dimensions and shape). The batch-to-batch fabrication reproducibility of the sensors and the sensing reproducibility between channels were assessed by analyzing the reflectance spectra of 15 chips from three different fabrication batches in random sensing areas and the reflectance spectra of different solutions HCl in water in a random chip flowed over the six sensing channels. Analyzing the reflectance spectra presented in S3A, the centroid of the plasmonic band has a mean value of 625.98 ± 0.61 nm with a coefficient of variation of only 0.1%. It can be observed in the figure a very low dispersion in the centroid of the plasmonic band for the 15 samples.

Furthermore, Figure 3E shows the six calibration curves obtained by flowing different HCl solutions over the six sensing channels at 40° (incidence angle of light), achieving a bulk refractive index sensitivity of 330.29 ± 5.35 nm/RIU with a coefficient of variation below 2%. Overall, the high-throughput fabrication process of Blu-ray discs at an industrial scale and the simple fabrication process of the plasmonic nanocrystals contribute to the achievement of highly reproducible substrates. The low coefficient of variation between fluidic channels offers a high potential platform for performing multichannel or multiplexed sensing assays. The sensing performance experimental results versus incident angle of light are summarized in Figure 3F. As can be observed in Figure 3F the plots have similar behavior to those obtained by FDTD simulations, with a decrease of the FWHM and biodetection performance and an increase in bulk refractive index sensitivity with high incident angles of light. As we mentioned before, to estimate the
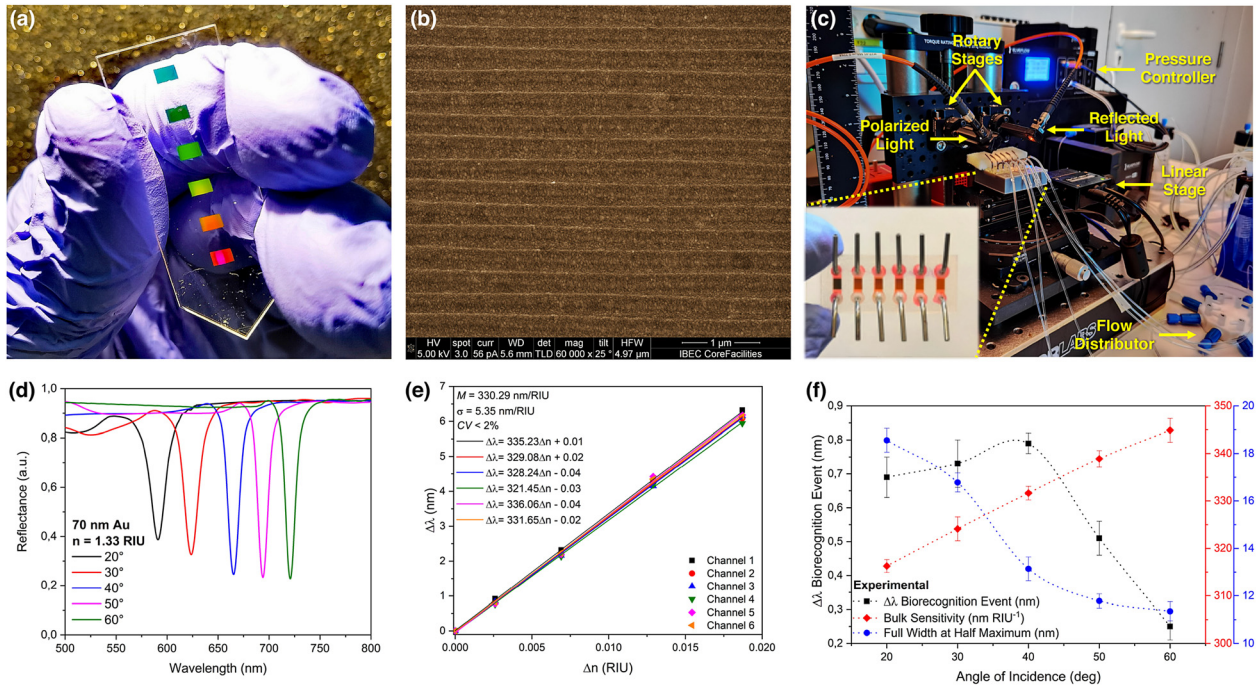
Figure 3: Fabrication and characterization of the multichannel 1D plasmonic nanocrystals-based biosensor.
(a) Photography of a 70 nm Au evaporated Blu-Ray disc substrate and the characteristic diffraction of light. (b) SEM photograph of the fabricated plasmonic nanocrystals. (c) Experimental set-up including the optical detection scheme and the microfluidic system. The insert shows the multichannel integrated sensor. (d) Variation of the reflectance spectra in the water of the plasmonic nanocrystals under different light incidence angles. (e) Calibration curves and bulk sensitivity reproducibility between the six channels for the proposed plasmonic sensor. (f) Influence of the different incident angles of light in the sensing and biosensing performance of the plasmonic nanostructures.

optimal incident angle of light for biosensing (the incident angle of light with the highest plasmonic shift $\Delta\lambda$ after the biorecognition event), we used the insulin/anti insulin model using a fixed protein target concentration. The surface sensitivity at 40° was slightly higher than those obtained at 20 and 30° without a significant difference between them. However, the lowest standard deviation in the measurements was achieved at 40°. Considering the slightly improved surface sensitivity and the low standard deviation, 40° was selected as the incident angle of light for the subsequent measurements. The differences between the optical and experimental results can be related to the fact that nanocrystals are radial to the Blu-Ray disc's circumference, which could influence the plasmonic coupling [44]. The highest plasmonic shifts after binding were achieved at low incident angles of light (see Figure S3B) with an increase in $\Delta\lambda$ up to 3× at incident angles below 45° versus 60°; these results are in agreement with previous reports [42, 43]. We achieved a bulk sensitivity in a range between ≈315 (at 20°) to 345 (at 60°) nm/RIU, which is highly competitive and similar to those obtained with engineered plasmonic nanograting or nanocrystal-based sensors [19–21]. Finally, although the Blu-Ray disc-based nanocrystals have fixed

structural dimensions (height and period) limiting the tunability and performance considering that the grating depth affects the radiative loss and, as a consequence the plasmonic coupling [45, 46] when compared to other approaches, there are still opportunities to improve even more their potential for biosensing using other plasmonic materials such as graphene [47] and nanoporous gold [48], or using novel deposition techniques such as glanced angle deposition [49] to partially tune the geometry of the plasmonic nanostructures making them a powerful strategy for the development of fast, cost-effective, and high throughput plasmonic nanocrystal-based sensing devices.

3.2 Biosensing evaluation with the integrated platform

To assess the biosensing capabilities of the developed integrated plasmonic nanocrystals biosensor, we use an endotoxin stimulation assay in bioengineered 3D skeletal muscle tissues and detect the secretion of IL-6 by muscle cells. IL-6 is four times bigger than insulin, the core protein is ~20 kDa, and glycosylation accounts for 21−26 kDa of

natural IL-6 [50]. Optimal set-up conditions (70 nm gold layer thickness and 40° angle of incidence) for the biorecognition of this biomolecule size were taking into account.

We first biofabricated the 3D muscle microtissues using a photomold encapsulation protocol already developed in our group [7]. C2C12 myoblasts were encapsulated in micromolded GelMA-CMCMA hydrogels on top of PEGDA-coated coverslips (Figure 4A). Seven days after the induction of muscle differentiation, we check the correct alignment and fusion of muscle cells via phase-contrast microscopy (Figure 4B, C). Moreover, confocal microscopy confirmed the maturation of the bioengineered tissue after staining with the skeletal muscle marker sarcomeric alpha-actinin (SAA) (Figure 4D, E).

The 70 nm gold film layer nanostructured substrate was modified by forming a self-assembled monolayer (SAM) with a carboxylic acid. Carboxylic groups (–COOH) were activated employing the carbodiimide chemistry, which results in an NHS ester intermediate highly reactive

to primary amines (NH2) present in the IL-6 antibodies. The chemical procedure is well established, and it generates highly stable amide bonds. The immobilization was performed ex-situ. As has been previously reported, this immobilization can improve the final biodetection performance of the biosensors [51]. The detection of different concentrations of IL-6 protein spiked in DMEM cell culture media (from 0.1 to 500 ng/mL) was performed with an incident angle of light of 40°, and they showed an excellent spectral evolution under an additive assay (see Figure 5A). We were able to achieve a LOD of 0.03 ng/mL ($\approx$1.4 pM), and a working range (WR) of 0.19–417.47 ng/mL, respectively (see the calibration curve in Figure 5B). The achieved LOD of IL-6 is at least one order of magnitude lower than those previously obtained by conventional prism coupled plasmonic [24] and nanoplasmonic [25, 26] refractometric biosensing based on gold-capped nanopillars in direct and label-free assays, and similar to those obtained by electrochemical biosensing platforms using indirect detection (secondary antibody sandwich assay) in cell culture media
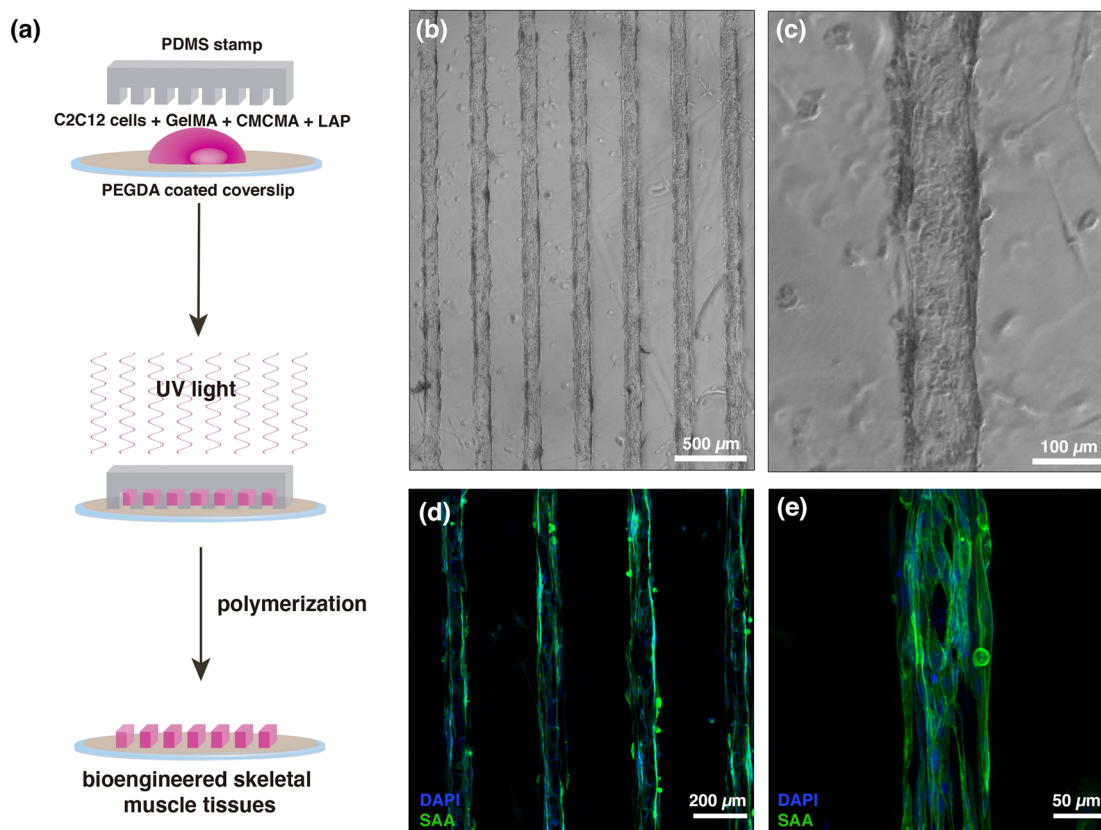

Figure 4: Bioengineered 3D skeletal muscles in GelMA hydrogels.
(a) Fabrication protocol to obtain 3D skeletal muscle tissues. hydrogels. A PDMS was used to fabricate cell-laden micropatterned GelMA-CMCMA hydrogels on top of PEGDA-coated glass coverslips by photopolymerization with UV light. (b–c) Microscope images of cell-laden micropatterned hydrogels. (d–e) Representative confocal microscopy images of 3D skeletal muscle microtissues stained for the muscle maturation marker sarcomeric α-actinin (SAA, green) and nuclei (DAPI, blue) after 10 days in differentiation conditions.

supernatants [4, 23]. Although the presented plasmonic biosensor has low sensitivity compared to those based on gold nanoparticles coated fiber optic [52] or those based on electrochemical silicon nanowires [53], we can remark two advantages: the presented plasmonic biosensor achieves direct and label-free biosensing in comparison with labeled indirect assay (fluorescent second antibody sandwich assay) presented on gold nanoparticles coated fiber-optic biosensors, and it is fabricated by a hight-throughput lithography-free method.

To induce the secretion of IL-6 by skeletal muscle tissues, we treated the 3D cultures with different concentrations of LPS for 48 h (Figure 5C). Then the supernatants of the treated tissues were analyzed using the plasmonic biosensor. We observed a dose-dependent increase in secreted IL-6 protein (Figure 5D). The supernatants of tissues that were not treated with LPS had a basal signal of IL-6 protein similar to the observed when analyzing the cell medium as a control (CNT). Therefore, and as it was

expected, there is no IL-6 secretion, but it is not induced with endotoxin treatment. Interestingly we detected a significant increase of secreted IL-6 by bioengineered tissues treated with LPS at 10 μg mL^{-1}. On a note, levels of IL-6 detected with our plasmonic biosensors were similar to previously reported endotoxin assays where IL-6 concentration was determined by ELISA or using electrochemical sensors [4, 23].

Finally, although ELISA is still the most common methodology used to determine relevant biomarkers in cell culture media [54], ELISA needs label detection, usually by secondary or sandwich reaction with time-consuming multiple steps and reagents [55]. Therefore, the potential for a direct, label-free, and real-time quantification of biomarkers in cell culture media can be highly valued to monitor the segregation of biomarkers from bioengineered 3D tissues or organoids and their dynamics to drugs or physical/chemical stimulus. The proposed nanostructured plasmonic biosensor provides a fast and reproducible
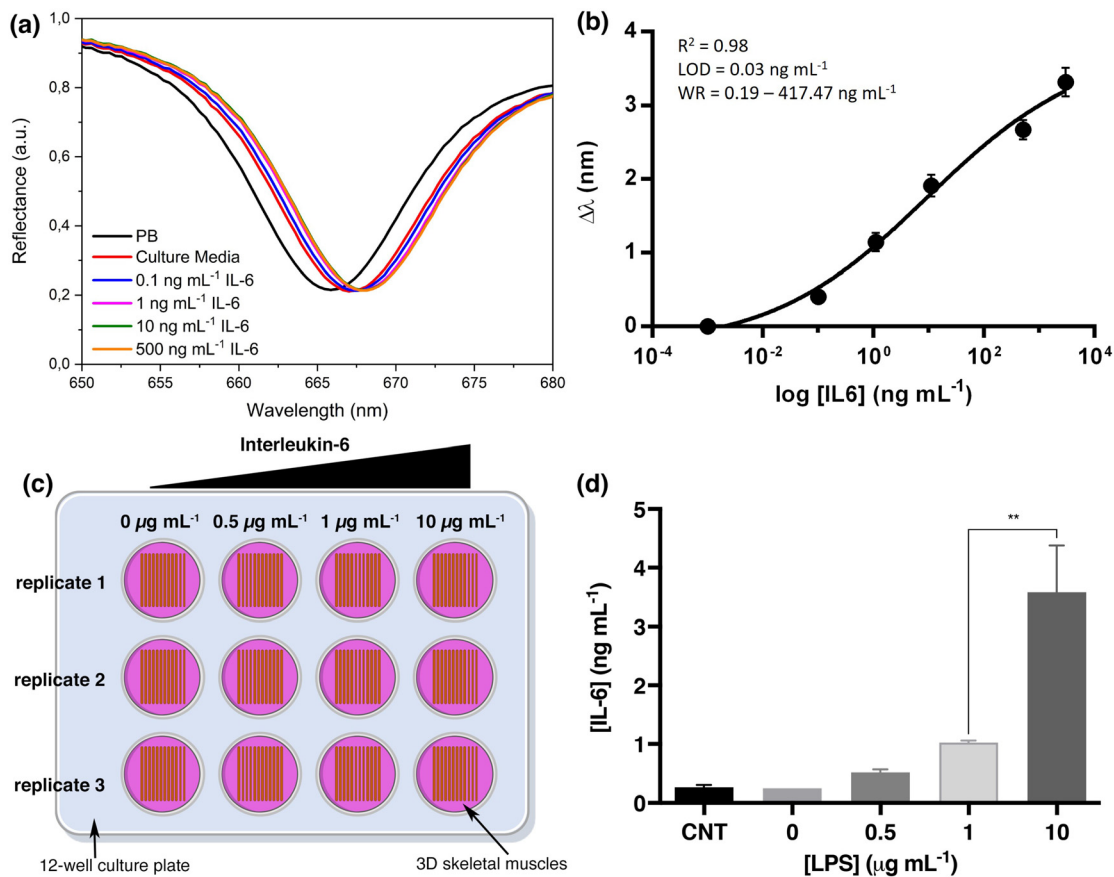

Figure 5: IL-6 biodetection in 3D skeletal muscle supernatants by 1D plasmonic nanocrystals.
(a) Plasmonic band displacement with different concentrations of spiked cell culture media in an additive assay. (b) Calibration curve for the detection of the IL-6 in cell culture media supernatants (n = 2). (c) Schematic representation of the stimulation assay of 3D skeletal muscle tissues with different concentrations of endotoxins. (d) IL-6 secretion changes with the concentration of endotoxins.

fabrication and a high biosensing performance in cell culture media while minimizing the optical set-up complexity being unnecessary using prism coupling. Overall, these results reflect the promising performance of these high throughput plasmonic nanostructures, with high potential to implement competitive devices for direct, label-free, and real-time quantification of biomarkers from bioengineered 3D tissues or organoids. Future efforts will be focused on real-time and multiplexed biosensing for developing monitoring platforms for cell cultures.

4 Conclusions

This work has developed high throughput and sensitive multichannel nanostructured plasmonic biosensor based on industrially produced Blu-ray as 1D nanocrystals containing substrates. By optimizing the metallic film thickness and incident angle of light, an improvement of up to 3× in biosensing experiments was achieved. In contrast to other engineered plasmonic crystals, we took advantage of the industrial scale fabricated 1D nanocrystals present in Blu-ray optical discs to achieve highly reproducible multichannel sensor chips batch to batch. The nanostructured plasmonic biosensors allowed us to monitor IL-6 secretion over time to a chemical stimulus based on different concentrations of endotoxins (lipopolysaccharides) in an *in vitro* bioengineered 3D skeletal muscles model. The nanostructured plasmonic biosensor represents a valuable tool to study the biomarker segregation to chemical stimulus *in vitro*. A LOD in the pM order in the undiluted cell culture supernatant was achieved without amplifying or pretreatment of the sample. Due to its high versatility and straightforward integration in organ-on-a-chip platforms, the presented plasmonic nanomaterial is an exciting candidate for developing sensing platforms for cell cultures.

References

[1] D. C. Christodouleas, B. Kaur, and P. Chorti, "From point-of-care testing to eHealth diagnostic devices (eDiagnostics)," *ACS Cent. Sci.*, vol. 4, pp. 1600–1616, 2018.

[2] F. Chiavaioli, P. Zubiate, I. Del Villar, et al., "Femtomolar detection by nanocoated fiber label-free biosensors," *ACS Sens.*, vol. 3, pp. 936–943, 2018.

[3] F. Chiavaioli, F. Baldini, S. Tombelli, C. Trono, and A. Giannetti, "Biosensing with optical fiber gratings," *Nanophotonics*, vol. 6, pp. 663–679, 2017.

[4] A. Hernández-Albors, A. G. Castaño, X. Fernández-Garibay, M. A. Ortega, J. Balaguer, and J. Ramón-Azcón, "Microphysiological sensing platform for an in-situ detection of tissue-secreted cytokines," *Biosens. Bioelectron. X*, vol. 2, p. 100025, 2019.

[5] V. Velasco, S. A. Shariati, and R. Esfandyarpour, "Microtechnology-based methods for organoid models," *Microsyst. Nanoeng.*, vol. 6, pp. 1–13, 2020.

[6] J. M. Fernández-Costa, X. Fernández-Garibay, F. Velasco-Mallorquí, and J. Ramón-Azcón, "Bioengineered in vitro skeletal muscles as new tools for muscular dystrophies preclinical studies," *J. Tissue Eng.*, vol. 12, 2021, 2041731420981339.

[7] X. Fernández-Garibay, M. A. Ortega, E. Cerro-Herreros, et al., "Bioengineered in vitro 3D model of myotonic dystrophy type 1 human skeletal muscle," *Biofabrication*, vol. 13, 2021, Art no. 035035.

[8] A. Henseleit, C. Pohl, T. Bley, and E. Boschke, "Monitoring human serum albumin cell cultures using surface plasmon resonance (SPR) spectroscopy," *J. Sens. Sens. Syst.*, vol. 4, pp. 77–83, 2015.

[9] G. A. Lopez, M. C. Estevez, M. Soler, and L. M. Lechuga, "Recent advances in nanoplasmonic biosensors: applications and lab-on-a-chip integration," *Nanophotonics*, vol. 6, pp. 123–136, 2017.

[10] E. C. Peláez, M. C. Estevez, A. Portela, J. P. Salvador, M. P. Marco, and L. M. Lechuga, "Nanoplasmonic biosensor device for the monitoring of acenocoumarol therapeutic drug in plasma," *Biosens. Bioelectron.*, vol. 119, pp. 149–155, 2018.

[11] B. Špačková, M. L. Ermini, and J. Homola, "High-performance biosensor exploiting a light guidance in sparse arrays of metal nanoparticles," *Opt. Lett.*, vol. 44, p. 1568, 2019.

[12] K. V. Sreekanth, M. ElKabbash, Y. Alapan, et al., "Hyperbolic metamaterials-based plasmonic biosensor for fluid biopsy with single molecule sensitivity," *EPJ Appl. Metamat.*, vol. 4, p. 1, 2017.

[13] O. Yavas, S. S. Aćimović, J. Garcia-Guirado, et al., "Self-calibrating on-chip localized surface plasmon resonance sensing for quantitative and multiplexed detection of cancer markers in human serum," *ACS Sens.*, vol. 3, pp. 1376–1384, 2018.

[14] J. Li, J. Ye, C. Chen, et al., "Biosensing using diffractively coupled plasmonic crystals: the figure of merit revisited," *Adv. Opt. Mater.*, vol. 3, pp. 176–181, 2015.

[15] J. Li, J. Ye, C. Chen, et al., "Revisiting the surface sensitivity of nanoplasmonic biosensors," *ACS Photonics*, vol. 2, pp. 425–431, 2015.

[16] F. Chiavaioli, C. A. Gouveia, P. A. Jorge, and F. Baldini, "Towards a uniform metrological assessment of grating-based optical fiber sensors: from refractometers to biosensors," *Biosensors*, vol. 7, p. 23, 2017.

[17] F. Liu, X. Zhang, K. Li, T. Guo, A. Ianoul, and J. Albert, "Discrimination of bulk and surface refractive index change in plasmonic sensors with narrow bandwidth resonance combs," *ACS Sens.*, vol. 6, pp. 3013–3023, 2021.

[18] G. A. López-Muñoz, M. C. Estevez, E. C. Peláez-Gutierrez, et al., "A label-free nanostructured plasmonic biosensor based on Blu-ray discs with integrated microfluidics for sensitive biodetection," *Biosens. Bioelectron.*, vol. 96, pp. 260–267, 2017.

[19] M. A. Ali, S. Tabassum, Q. Wang, Y. Wang, R. Kumar, and L. Dong, "Integrated dual-modality microfluidic sensor for biomarker detection using lithographic plasmonic crystal," *Lab Chip*, vol. 18, pp. 803–817, 2018.

[20] A. E. Cetin and S. N. Topkaya, "Photonic crystal and plasmonic nanohole based label-free biodetection," *Biosens. Bioelectron.*, vol. 132, pp. 196–202, 2019.

[21] K. L. Lee, M. L. You, X. Shi, et al., "Injection compression molding of transmission-type Fano resonance biochips for multiplex sensing applications," *Appl. Mater. Today*, vol. 16, pp. 72–82, 2019.

[22] R. A. Frost and C. H. Lang, "Skeletal muscle cytokines: regulation by pathogen-associated molecules and catabolic hormones," *Curr. Opin. Clin. Nutr. Metab. Care*, vol. 8, pp. 255–263, 2005.

[23] M. A. Ortega, X. Fernández-Garibay, A. G. Castaño, et al., "Muscle-on-a-chip with an on-site multiplexed biosensing system for: in situ monitoring of secreted IL-6 and TNF-α," *Lab Chip*, vol. 19, pp. 2568–2580, 2019.

[24] T. H. Chou, C. Y. Chuang, and C. M. Wu, "Quantification of Interleukin-6 in cell culture medium using surface plasmon resonance biosensors," *Cytokine*, vol. 51, pp. 107–111, 2010.

[25] X. Luo, C. Zhu, M. Saito, et al., "Cauliflower-like nanostructured localized surface plasmon resonance biosensor chip for cytokine detection," *Bull. Chem. Soc. Jpn.*, vol. 93, pp. 1121–1126, 2020.

[26] C. Zhu, X. Luo, W. V. Espulgar, et al., "Real-time monitoring and detection of single-cell level cytokine secretion using LSPR technology," *Micromachines*, vol. 11, pp. 2–11, 2020.

[27] G. A. López-Muñoz, M. C. Estévez, M. Vázquez-García, et al., "Gold/silver/gold trilayer films on nanostructured polycarbonate substrates for direct and label-free nanoplasmonic biosensing," *J. Biophotonics*, vol. 11, 2018, Art no. e201800043.

[28] N. Sultanova, S. Kasarova, and I. Nikolov, "Dispersion properties of optical polymers," *Acta Phys. Pol, A*, vol. 116, pp. 585–587, 2009.

[29] M. Wakaki, K. Kudo, and T. Shibuya, *Physical Properties and Data of Optical Materials 2007*, Boca Raton, FL, CRC Press.

[30] Y. Xu, P. Bai, X. Zhou, et al., "Optical refractive index sensors with plasmonic and photonic structures: promising and inconvenient truth," *Adv. Opt. Mater.*, vol. 7, pp. 31–33, 2019.

[31] A. García-Lizarribar, X. Fernández-Garibay, F. Velasco-Mallorquí, A. G. Castaño, J. Samitier, and J. Ramon-Azcon, "Composite biomaterials as long-lasting scaffolds for 3D bioprinting of highly aligned muscle tissue," *Macromol. Biosci.*, vol. 18, p. 1800167, 2018.

[32] A. Oubiña, B. Ballesteros, P. B. Carrasco, R. Galve, J. Gascón, F. Iglesias, N. Sanvicens, and M. P. Marco, "Immunoassays for environmental analysis," in *Techniques and Instrumentation in Analytical Chemistry*, vol. 21, D BarcelÓ, Ed, Elsevier, 2000, pp. 287–339.

[33] F. Chiavaioli, C. Trono, A. Giannetti, M. Brenci, and F. Baldini, "Characterisation of a label-free biosensor based on long period grating," *J. Biophotonics*, vol. 7, pp. 312–322, 2014.

[34] H. P. Erickson, "Size and shape of protein molecules at the nanometer level determined by sedimentation, gel filtration, and electron microscopy," *Biol. Proced. Online*, vol. 11, pp. 32–51, 2009.

[35] P. R. Shorten, C. D. McMahon, and T. K. Soboleva, "Insulin transport within skeletal muscle transverse tubule networks," *Biophys. J.*, vol. 93, pp. 3001–3007, 2007.

[36] Y. H. Tan, M. Liu, B. Nolting, J. G. Go, J. Gervay-Hague, and G. Y. Liu, "A nanoengineering approach for investigation and regulation of protein immobilization," *ACS Nano*, vol. 2, pp. 2374–2384, 2008.

[37] J. Li, C. Chen, L. Lagae, and P. van Dorpe, "Nanoplasmonic sensors with various photonic coupling effects for detecting different targets," *J. Phys. Chem. C*, vol. 119, pp. 29116–29122, 2015.

[38] K. L. Lee, C. C. Chang, M. L. You, M. Y. Pan, and P. K. Wei, "Enhancing the surface sensitivity of metallic nanostructures using oblique-angle-induced fano resonances," *Sci. Rep.*, vol. 6, pp. 1–13, 2016.

[39] A. Sinibaldi, V. Montaño-Machado, N. Danz, et al., "Real-time study of the adsorption and grafting process of biomolecules by means of Bloch surface wave biosensors," *ACS Appl. Mater. Interfaces*, vol. 10, pp. 33611–33618, 2018.

[40] V. G. Kravets, A. Kabashin, W. L. Barnes, and A. N. Grigorenko, "Plasmonic surface lattice resonances: a review of properties and applications," *Chem. Rev.*, vol. 118, pp. 5912–5951, 2018.

[41] W. Zhou and T. W. Odom, "Tunable subradiant lattice plasmons by out-of-plane dipolar interactions," *Nat. Nanotechnol.*, vol. 6, pp. 423–427, 2011.

[42] H. Gao, J. C. Yang, J. Y. Lin, et al., "Using the angle-dependent resonances of molded plasmonic crystals to improve the sensitivities of biosensors," *Nano Lett.*, vol. 10, pp. 2549–2554, 2010.

[43] J. Y. Lin, A. D. Stuparu, M. D. Huntington, M. Mrksich, and T. W. Odom, "Nanopatterned substrates increase surface

sensitivity for real-time biosensing," *J. Phys. Chem. C*, vol. 117, pp. 5286–5292, 2013.

[44] F. Romanato, K. H. Lee, G. Ruffato, and C. C. Wong, "The role of polarization on surface plasmon polariton excitation on metallic gratings in the conical mounting," *Appl. Phys. Lett.*, vol. 96, p. 111103, 2010.

[45] S. Rossi, E. Gazzola, P. Capaldo, G. Borile, and F. Romanato, "Grating-coupled surface plasmon resonance (GC-SPR) optimization for phase-interrogation biosensing in a microfluidic chamber," *Sensors*, vol. 18, p. 1621, 2018.

[46] J. S. Yuk, E. F. Guignon, and M. A. Lynes, "Sensitivity enhancement of a grating-based surface plasmon-coupled emission (SPCE) biosensor chip using gold thickness," *Chem. Phys. Lett.*, vol. 591, pp. 5–9, 2014.

[47] X. Xiong, Y. Chen, H. Wang, et al., "Plasmonic interface modified with graphene oxide sheets overlayer for sensitivity enhancement," *ACS Appl. Mater. Interfaces*, vol. 10, pp. 34916–34923, 2018.

[48] N. Kim, M. Choi, J. W. Leem, et al., "Improved biomolecular detection based on a plasmonic nanoporous gold film fabricated by oblique angle deposition," *Opt. Express*, vol. 23, p. 18777, 2015.

[49] B. Chen, A. Wood, A. Pathak, et al., "Plasmonic gratings with nano-protrusions made by glancing angle deposition for single-molecule super-resolution imaging," *Nanoscale*, vol. 8, pp. 12189–12201, 2016.

[50] T. Tanaka, M. Narazaki, and T. Kishimoto, "IL-6 in inflammation, immunity, and disease," *Cold Spring Harb. Perspect. Biol.*, vol. 6, p. a016295, 2014.

[51] M. Soler, M. C. Estevez, M. Alvarez, M. Otte, B. Sepulveda, and L. Lechuga, "Direct detection of protein biomarkers in human fluids using site-specific antibody immobilization strategies," *Sensors*, vol. 14, pp. 2239–2258, 2014.

[52] G. Liu, K. Zhang, A. Nadort, M. R. Hutchinson, and E. M. Goldys, "Sensitive cytokine assay based on optical fiber allowing localized and spatially resolved detection of interleukin-6," *ACS Sens.*, vol. 2, pp. 218–226, 2017.

[53] D. Rani, Y. Singh, M. Salker, X. T. Vu, S. Ingebrandt, and V. Pachauri, "Point-of-care-ready nanoscale ISFET arrays for sub-picomolar detection of cytokines in cell cultures," *Anal. Bioanal. Chem.*, vol. 412, pp. 6777–6788, 2020.

[54] Y. C. E. Li and I. Chi Lee, "The current trends of biosensors in tissue engineering," *Biosensors*, vol. 10, p. 88, 2020.

[55] M. Beeg, A. Nobili, B. Orsini, et al., "A Surface Plasmon Resonance-based assay to measure serum concentrations of therapeutic antibodies and anti-drug antibodies," *Sci. Rep.*, vol. 9, pp. 1–9, 2019.